Electronic Supplementary Material (ESI) for Journal of Materials Chemistry C.

Supporting Information

Sculptured Thin Film Vanadium dioxide Thermochromic Coatings Grown by Oblique Angle Deposition: Investigation of Transmittance Response and Modulation Enhancement by Experiment and Theoretical Modeling

Saranya Bhupathi,[a,b] Mohammad Abutoama,[c] Yi Long,[a,b] Ibrahim Abdulhalim[a,b,c*]*

[a] School of Materials Science and Engineering, Nanyang Technological University, 50 Nanyang Avenue, 639798, Singapore.

[b] Singapore-HUJ Alliance for Research and Enterprise (SHARE), Nanomaterials for Energy and Energy-Water Nexus (NEW), Campus for Research Excellence and Technological Enterprise (CREATE), 138602, Singapore.

[c] Department of Electro-optics and Photonics Engineering, School of Electrical and Computer Engineering, Ben-Gurion University of the Negev, Beer Sheva, 84105, Israel.

[*] Authors for correspondence. E-mail: abdulhlm@bgu.ac.il and E-mail: longyi@ntu.edu.sg

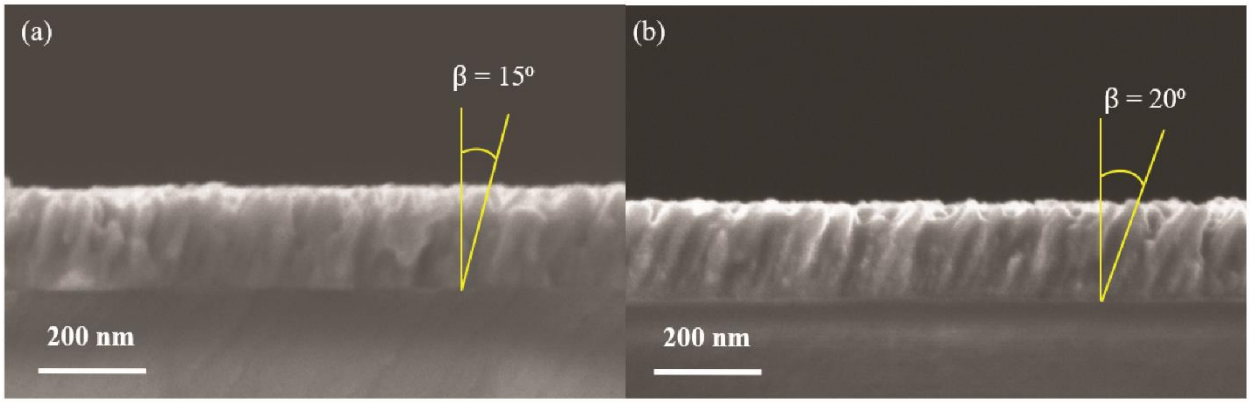

Fig. S1 SEM cross-section images of the as-prepared STF vanadium at the deposition angles (b) $\alpha = 70°$ and (b) $\alpha = 80°$.

Table S1. Summary of the AFM average roughness of as-prepared STF vanadium and STF VO_2 annealed at different temperatures and times

Sample code	Annealing	Annealing temperature (°C)	Annealing time (min)	Average roughness (nm)
T1	No (as-prepared sample)	-	-	2.5
T2	Yes	400	2	5.8
T3	Yes	450	2	9.5
T4	Yes	500	2	10.3
T5	Yes	450	4	8.8
T6	Yes	450	6	9.8
T7	Yes	450	8	10.0
T8	Yes	450	10	9.8

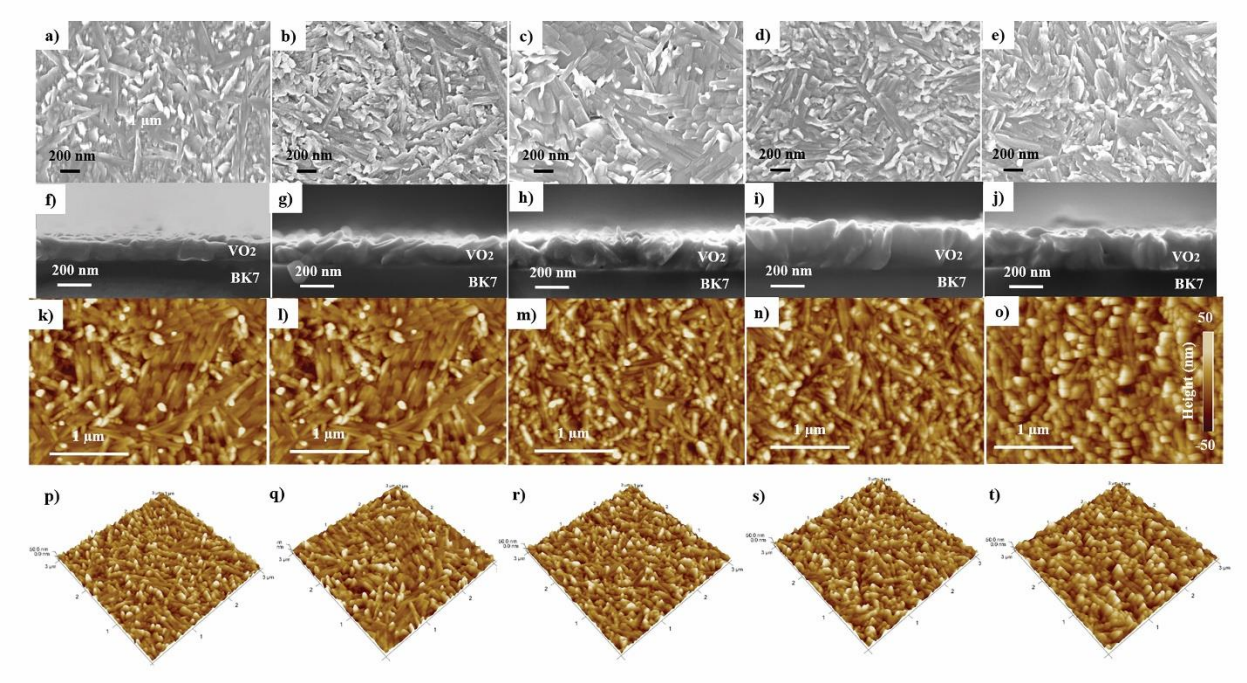

Fig. S2 SEM top-view images of the samples (a) T3 (b) T5 (c) T6 (d) T7 and (e) T8. SEM cross-section images of the samples (f) T3 (g) T5 (h) T6 (i) T7 and (j) T8. AFM 2D pictures of the samples (k) T3 (l) T5 (m) T6 (n) T7 and (o) T8. AFM 3D pictures of the samples (p) T3 (q) T5 (r) T6 (s) T7 and (t) T8. T3, T5, T6, T7, and T8 are the heat-treated samples having different annealing times maintaining a constant annealing temperature. The oxidation annealing times of the samples T3, T5, T6, T7, and T8 are 2, 4, 6, 8, and 10 min respectively, with a constant annealing temperature of 450 °C in the ambient air.

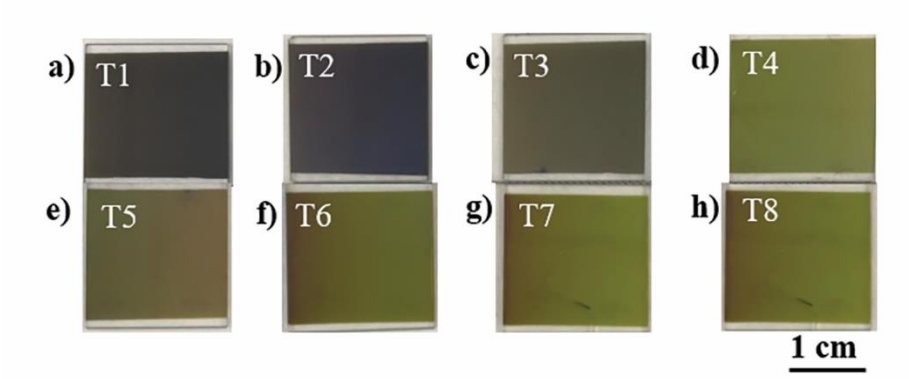

Fig. S3 Photograph of the samples (a) T1 (b) T2 (c) T3 (d) T4 (e) T5 (f) T6 (g) T7 and (h) T8.

The sample T1 corresponds to as-prepared STF vanadium, whereas the samples T2 to T8 are the samples subjected to different heat-treatments having different annealing temperatures and times. The oxidation annealing temperatures of the samples T2, T3, and T4 are 400, 450, and 500 ºC respectively, with a constant annealing time of 2 min in the ambient air. The oxidation annealing times of the samples T5, T6, T7 and T8 are 4, 6, 8 and 10 min respectively, with a constant annealing temperature of 450 ºC in the ambient air. It is known that VO_2 is sensitive to air and prone to degradation when exposed to ambient air.[1,2,3] The color variation on the sample surface could be due to the presence of different oxides of vanadium[4] as a result of surface oxidation, after prolonged exposure of samples in the ambient air for various characterizations. A thickness variation of 8 to 12% is noticed at the sample edges that happens when the substrate is placed at an oblique angle for the deposition. The color changes particularly at the edges could also be due to the thickness variation in the sample edges.

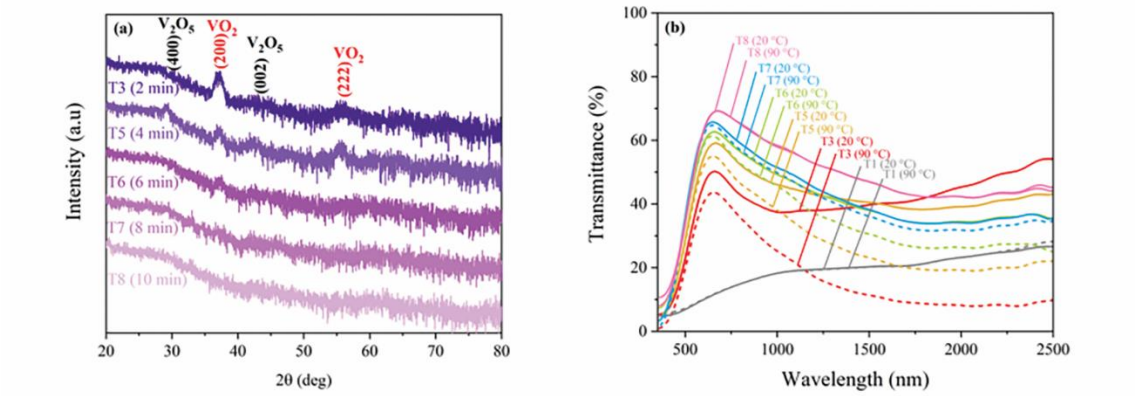

Fig. S4 (a) GIXRD patterns corresponding to the samples T3, T5, T6, T7, and T8 for 2θ ranging from 20 to 80 degrees. (b) Transmittance responses of the samples T1, T3, T5, T6, T7, and T8 under unpolarized light at the measurement temperatures 20 and 90 °C. The sample T1 corresponds to as-prepared STF vanadium, whereas T3, T5, T6, T7, and T8 are the samples subjected to different heat treatments. The oxidation annealing times of the samples T3, T5, T6, T7, and T8 are 2, 4, 6, 8, and 10 min respectively, with a constant annealing temperature of 450 ºC in the ambient air.

Table S2. Comparison of the thermochromic performance of VO_2 thin films (grown by various techniques, different substrates, and thicknesses) with the present work

Sample	Substrate	Fabrication method	Thickness	Deposition configuration	$T_{lum(avg)}$ (%)	$\Delta T_{ir(2000\ nm)}$ (%)	ΔT_{sol} (%)
VO_2 single layer	Quartz[5]	PVD	130 nm	normal	39.7	45.1	10.2
	BK7[6]	DC sputtering	90 nm	normal	35.4		9.7
	BK7[7]	Reactive sputtering	50 nm	normal	37.3	44.4	6.1
	Soda-lime[8]	HiPIMS	95 nm	normal	24.4		8.8
	HT glass[8]	HiPIMS	95 nm	normal	22.0		10.6
	Quartz[8]	HiPIMS	95 nm	normal	19.3		12.2
	Soda-lime[9]	HiPIMS	88 nm	normal	30.5	37.0	4.0
	Fused Quartz[10]	Sol-gel	65 nm	normal	68.2	30.0	4.6
	Float glass[11]	RF sputtering	120 nm	normal	24.8	25.6	4.6
	Fused silica[11]	RF sputtering	90 nm	normal	37.7	27.7	4.0
	Glass[12]	Reactive sputtering	100 nm	normal	41.5		6.9
	Glass[13]	CVD	300 nm	normal	15.4		3.1
STF VO_2 (This work)	BK7	RF sputtering	130 nm	oblique angle (α = 85°)	41.2	37.3	8.9

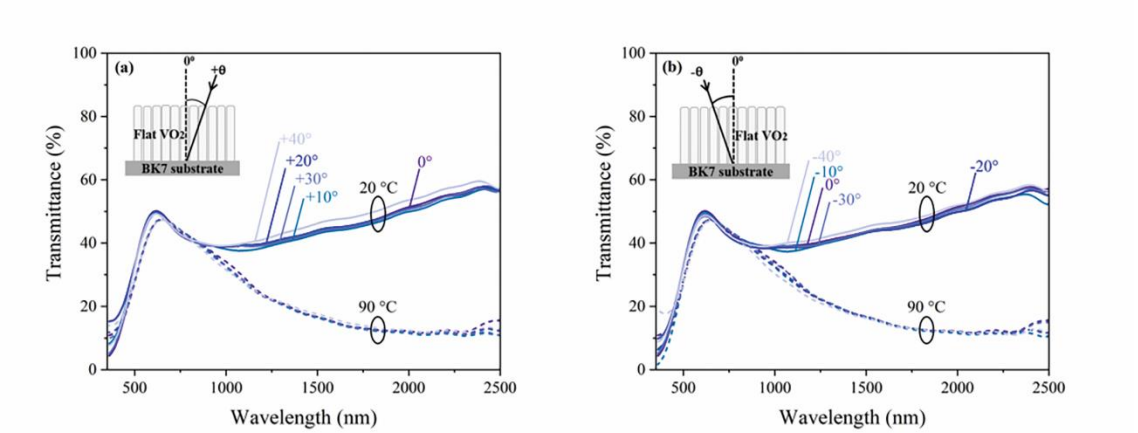

Fig. S5 Angular transmittance responses of flat VO_2 under unpolarized light at the measurement temperatures 20 and 90 °C (a) for the positive angles of incidence from +10° to +40° and (b) for the negative angles of incidence from -10° to -40° (in steps of 10°) with respect to 0°, where 0º is the measurement in the normal incidence. The insets in (a) and (b) are the schematics of the transmittance measurements for the positive and negative angles of incidence respectively in flat VO_2 with straight nanocolumns. The dotted lines in the inset indicate the substrate normal, and the arrow indicates the light ray.

Table S3. Comparison of thermochromic performance of recent work on STF VO_2 (transmittance measured in normal and oblique incidence) with the present work

Sample	Substrate	Fabrication method	Thickness	Deposition configuration	Tilt angle (β)	Light incidence angle	$T_{lum(avg)}$ (%)	ΔT_{nir} (%)	ΔT_{sol} (%)
STF VO_2 (This work)	BK7	RF sputtering	130 nm	oblique angle (α = 85º)	20º	0º	41.2	7.0	8.9
						+30º	40.8	7.2	9.6
						-30º	39.3	6.5	8.4
STF VO_2	BK7[14]	Thermal evaporation	≈500 nm	oblique angle (α = 85º)	47º	0º	33.8		6.4
						+30º	32.4		7.0
						-30º	34.4		6.1

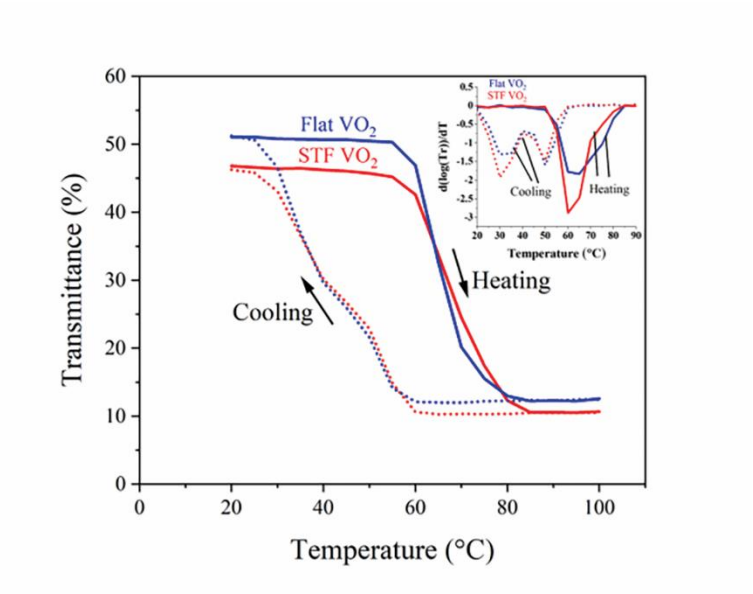

Fig. S6 Transmittance hysteresis loop of STF VO_2 and flat VO_2 at the wavelength of 2000 nm. The black arrows indicate heating and cooling directions. The inset shows the transmittance derivative curves of STF VO_2 and flat VO_2 versus the measurement temperature.

Table S4. Summary of thermal hysteresis characteristics of STF VO_2 and flat VO_2

Sample	T_c in heating and cooling branches (°C)		T_c (°C)	ΔT_c (°C)
	$T_{c(heating)}$	$T_{c(cooling)}$		
STF VO_2	65	30/50	47.5/57.5	35/15
Flat VO_2	60	30/50	45/55	30/10

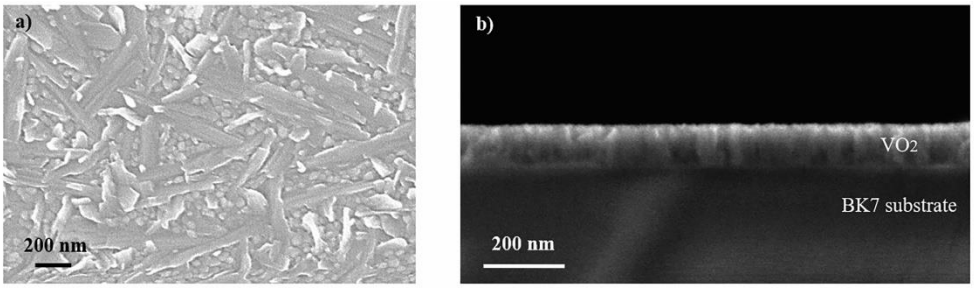

Fig. S7 SEM (a) top-view and (b) cross-section images of flat VO_2 annealed at 450 ºC for 2 min.

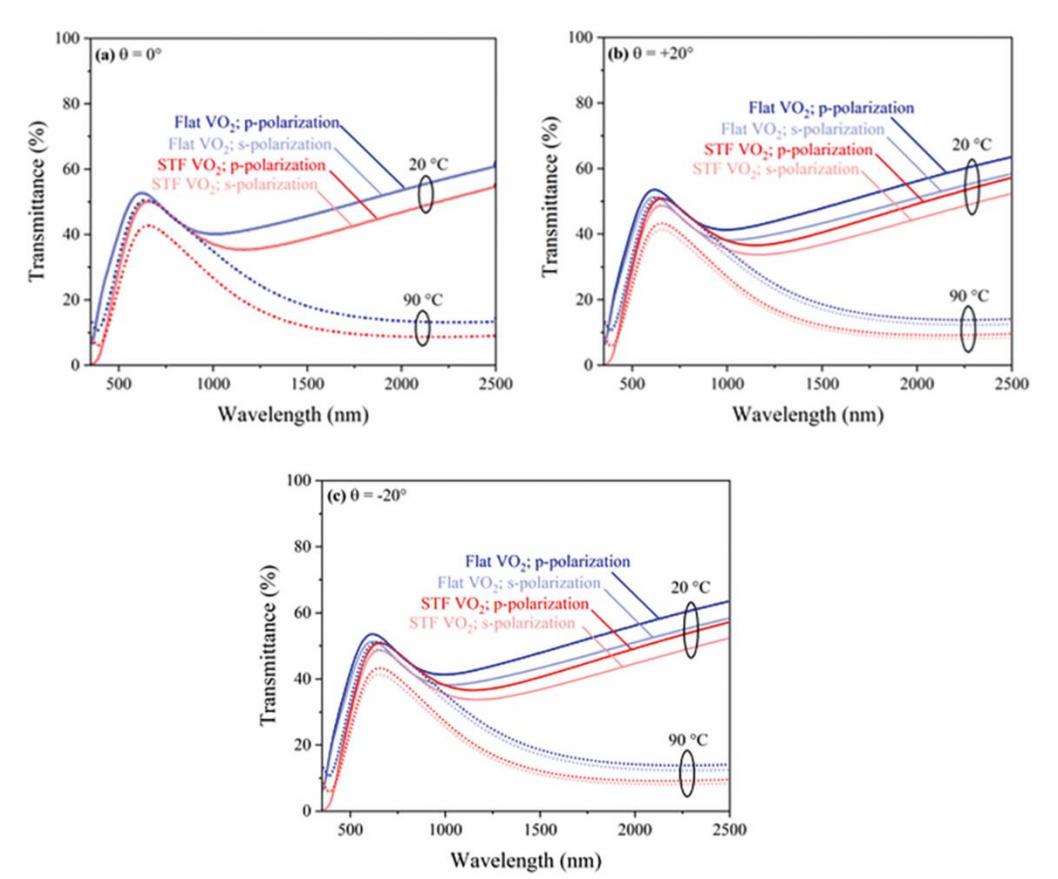

Fig. S8 Polarization (s and p-polarizations) dependence of the transmittance spectra at both 20 and 90 ºC for the flat and STF VO_2 samples at (a) θ = 0º (b) θ = +20º (c) θ = -20º. The thickness of both flat and STF VO_2 is 130 nm, while f_a of STF VO_2 is 89%.

References

[1] L. Chen, X. Wang, D. Wan, Y. Cui, B. Liu, S. Shi, H. Luo and Y. Gao, *RSC Adv.*, 2016, **6**, 73070.

[2] T. Chang, X. Cao, N. Li, S. Long, Y. Zhu, J. Huang, H. Luo and P. Jin, *Matter*, 2019, **1**, 734–744.

[3] X. Wang, Y. Cao, C. Yang, L. Yan and Y. Li, *J. Vac. Sci. Technol., A*, 2016, **A34**, 01A106.

[4] Y. B. Kang, *J. Eur. Ceram. Soc.*, 2012, **32**, 3187–3198.

[5] S. Bhupathi, S. Wang, M. Abutoama, I. Balin, L. Wang, P. G. Kazansky, Y. Long and I. Abdulhalim, *ACS Appl. Mater. Interfaces*, 2020, **12**, 41905−41918.

[6] Y. Yang, X. Cao, G. Sun, S. Long, T. Chang, X. Li and P. Jin, *J. Alloys Compd.*, 2019, **791**, 648-654.

[7] S. Long, H. Zhou, S. Bao, Y. Xin, X. Cao and P. Jin, *RSC Adv.*, 2016, **6**, 106435.

[8] T. D. Vu, S. Liu, X. Zeng, C. Li and Y. Long, *Ceram. Int.*, 2020, **46**, 8145–8153.

[9] J. Houska, D. Kolenaty, J. Vlcek and R. Cerstvy, *Thin Solid Films* 2018, **660**, 463–470.

[10] C. Wang, L. Zhao, Z. Liang, B. Dong, L. Wan and S. Wang, *Sci. Technol. Adv. Mater.*, 2017, **18**, 563-573.

[11] E. Gagaoudakis, E. Aperathitis, G. Michail, G. Kiriakidis and V. Binas, *Sol. Energy Mater. Sol. Cells*, 2021, **220**, 110845.

[12] S. Long, X. Cao, Y. Wang, T. Chang, N. Li, L. Jin, L. Ma, F. Xu, G. Sun and P. Jin, *Sol. Energy Mater. Sol. Cells*, 2020, **209**, 110449.

[13] M. J. Powell, R. Q.-Cabrera, A. Taylor, D. Teixeira, L. Papakonstantinou, R. G. Palgrave, G. Sankar and I. P. Parkin, *Chem. Mater.*, 2016, **28**, 1369-1376.

[14] Y. Sun, X. Xiao, G. Xu, G. Dong, G. Chai, H. Zhang, P. Liu, H. Zhu and Y. Zhan, *Sci. Rep.*, 2013, **3**, 2756.